

Characterization of European sprat acoustic backscatter through modeling techniques: A comparison with *in situ* observations in the Mediterranean Sea

Antonio Palermino^a, Sven Gastauer^b, Andrea De Felice^a, Giovanni Canduci^a, Ilaria Biagiotti^a, Iole Leonori^{a,*} 

^a CNR-National Research Council, IRBIM-Institute for Marine Biological Resources and Biotechnology, Largo Fiera della Pesca, 2, 60125 Ancona, Italy

^b Thünen Institute of Sea Fisheries, Bremerhaven, Germany

ARTICLE INFO

Keywords:

Target strength
Fisheries acoustics
Broadband
Modeling
Swim bladder
Sprat
Mediterranean Sea

ABSTRACT

In fisheries acoustics, the identification of targets and the precise conversion of acoustic energy into biologically important meaningful metrics remain a challenge. Backscattering cross-section, or its logarithmic form, Target Strength (TS, dB re 1 m²), is a key parameter in this process. While numerous studies exist on the TS of commercially important species, there is a paucity of research on commercially ancillary species, such as the European sprat in the Mediterranean Sea, which is nonetheless of great importance for the pelagic ecosystem. The application of backscattering models can enhance our understanding of this species' acoustic properties. In this study, we applied several backscattering models on three-dimensional swim bladder shapes derived from Computer Tomography (CT) scans of sprat collected during the MEDiterranean International Acoustic Survey (MEDIAS). The theoretical TS pattern was compared with empirical empirically TS measurements, demonstrating a good fit at 38 and 70 kHz between 0° (broadside incidence) and -20°. Significant differences were observed at higher frequencies and tilt angles. This study provides estimates of the relative frequency response and broadband backscatter of sprat in the Mediterranean Sea. We proposed a new relevant TS to length relationship of 20 log(L)-68.3 dB re 1 m² at 38 kHz for European sprat in the Mediterranean Sea.

1. Introduction

Sprattus sprattus is the third most important species in terms of landings in the GFCM (General Fisheries Commission for the Mediterranean) region (FAO, 2023). In the Black Sea, it is targeted by purse seines and pelagic trawlers, while in the Western Mediterranean Sea and the Adriatic Sea, it holds low commercial value, contributing less than 1 % to pelagic trawl landings, as it is frequently discarded (FAO, 2023). Sprat holds an important role in the pelagic ecosystem, as an important predator for zooplankton and as an abundant prey resource for piscivorous species. In the Adriatic Sea it contributes to the equilibrium of the pelagic food web, competing with the two more abundant planktivorous species, *Engraulis encrasicolus* and *Sardina pilchardus* (Fanelli et al., 2023). However, rising sea temperatures threaten this cold-tolerant species, potentially leading to local extinction across the entire Mediterranean Sea (Schickele et al., 2021; Palermino et al., 2024). With regard to ecosystem-based management strategies, robust monitoring of

the sprat population in the Mediterranean Sea is of great importance (Schickele et al., 2021). Monospecific sprat schools are rare, they are more commonly observed in mixed aggregations, together with other clupeids, such as anchovies (Fernades et al., 2005). The annual abundance of sprat in the Mediterranean Sea is estimated by means of the MEDiterranean International Acoustic Survey (MEDIAS) (Leonori et al., 2021). Acoustic surveys provide high-resolution data across large spatial and temporal scales, partitioned into biological groups of interest. The collection of biological validation data remains indispensable for the correct assignment of acoustic backscatter to a single species, sex, and group. Advancements in fisheries acoustic technologies have enabled the utilization of a broad range of frequencies or broadband spectra as key tools for classification into species or other biologically meaningful groups (Stanton et al., 2010).

One of the main challenges in fisheries acoustics is the interpretation of collected data, identifying the targets, and converting acoustic energy into biologically meaningful metrics, such as density, abundance, or

* Corresponding author.

E-mail address: iole.leonori@cnr.it (I. Leonori).

<https://doi.org/10.1016/j.fishres.2025.107298>

Received 20 August 2024; Received in revised form 11 February 2025; Accepted 11 February 2025

Available online 16 February 2025

0165-7836/© 2025 The Author(s). Published by Elsevier B.V. This is an open access article under the CC BY license (<http://creativecommons.org/licenses/by/4.0/>).

biomass estimates (Simmonds and MacLennan, 2005). Measures of acoustic energy can be converted into numerical densities through the species-specific acoustic backscattering cross-section that is commonly expressed in its logarithmic form as target strength (TS, dB re 1 m²), which is a key parameter. For swim-bladdered fish species, TS is largely determined by swim bladder features (shape, size, and inflation), as well as on the acoustic frequency and tilt angle of the fish (Foote, 1987; Ona, 1990). The high level of stochasticity in TS estimates is one of the main sources of uncertainty in acoustic biomass estimates (Baird et al., 2022; Gastauer et al., 2017; O'Driscoll, 2004; Scouling et al., 2017). The relationship between TS and measured total fish length (L) is commonly expressed as (Simmonds and MacLennan, 2005):

$$TS = m \log_{10} L + b \quad (1)$$

or as proposed by Foote (1987):

$$TS = 20 \log_{10} L + b_{20} \quad (2)$$

Where the intercepts b or b_{20} can be interpreted as the TS normalized by L through a slope m in the first case and by the square of L in the second case. A slope of 20 assumes a proportional growth of the swim bladder relative to the square of fish length (Foote, 1987).

In situ empirical TS data are generally considered to provide the most reliable measurements capturing the fish within their natural environment and with their natural behavior (O'Driscoll et al., 2018; Salvat et al., 2020). A limitation of the *in situ* method is the presence of monospecific schools at a low enough density to enable the clear separation of individual fish (Sawada et al., 1993), typically not observed for sprat in the Mediterranean Sea (FAO, 2023). *Ex situ* experiments using live fish are seldom conducted on small clupeid species such as sprat due to being time-consuming and logistically challenging (Sobradillo et al., 2021). Alternatively, backscattering models provide a precise estimate of theoretical backscatter by utilizing a range of parameters, including information on the organism's anatomy, material properties, tilt angles, and acoustic frequencies. A gas-filled swim bladder, creates a strong acoustic boundary with an abrupt change in acoustic impedance, due to stark contrasts in density and sound speed compared to the surrounding body. As such, the swim bladder becomes the main source of backscatter for swim-bladdered fish (Foote, 1980). Fish swim bladders can have complex shapes and tilted positions that affect the backscatter. This effect can be amplified or reduced by fish orientation (tilt angle) (Membiela and dell'Erba, 2018; Reeder et al., 2004). Previous studies have demonstrated that the hepato-somatic index, gonad-somatic index, and stomach fullness influence swim bladder circularity, area, and relative size (Ganias et al., 2015; Ok and Gücü, 2019), hence impacting the backscattering cross-section of the fish. Moreover, in physostomous fish species, the volume of the swim bladder decreases with increasing ambient water pressure (Fässler and Gorska, 2009; Gorska and Ona, 2003).

A rich array of theoretical backscattering models have been developed since 1950 (Anderson, 1950; Jech et al., 2015). The simplest way to model a swim bladder is through a regular geometric shape, such as a sphere, a finite cylinder, or a prolate spheroid/ellipsoid, for which exact solutions can be found. Conversely, numerical or approximate models can be used to incorporate more complex and realistic 3D shapes. Such models require an accurate representation of swim bladder morphology, which can be obtained through dissection (Ayoubi et al., 2016) or X-ray scanning (Hazen and Horne, 2004; Horne, 2000; Jech et al., 2015). Even more detailed images can be obtained through computer tomography scans (CT) and magnetic resonance imaging (MRI) (Fässler et al., 2013; Gastauer et al., 2016). These techniques can be used to implement approximation models, including the Kirchhoff-Ray-Mode model (KRM) (Furusawa, 1988; Jech et al., 1995), along with complex numerical models that solve wave equations on finite surface elements, such as the Boundary Element Method (BEM) and the Finite Element Method (FEM) (Francis and Foote, 2003; O'Driscoll et al., 2011). Numerical models can

deal with any shape and material properties despite they can fails to very high frequencies due to numerical issues (Gonzalez et al., 2020). They are commonly available through several licensed and open-source software, including COMSOL Multiphysics (v. 6) (COMSOL, 2021), Coupled BEM in Julia (Gonzalez et al., 2020), or BEMPP in Python (Smigaj et al., 2015). The frequency response across a broad frequency range can potentially enhance the ability to distinguish between acoustically similar species and size groups of a single species (Benoit-Bird and Waluk, 2020; Kubilius et al., 2020).

Following the advent of transducers capable of transmitting frequency-modulated pulses (FM), several *in situ* studies have been conducted on pelagic fish (Bassett et al., 2018; Benoit-Bird and Waluk, 2020; Gugele et al., 2021). However, multi-frequency characterization of scattering targets remains more commonly used than broadband investigations for acoustic survey data analysis (Korneliusen and Ona, 2002; Fernandes et al., 2005; Korneliusen, 2018; MEDIAS, 2018).

Several studies have described the multi-frequency acoustic backscattering properties of clupeids and engraulidae species (De Felice et al., 2015; Fernandes et al., 2005), although few studies have examined the broadband backscatters of these species (Antona, 2016; Lavia et al., 2020). Antona (2016) was the sole researcher to investigate the broadband TS of herring and sprat in the North Sea using *in situ* data and theoretical modelling; several studies were conducted on sprat acoustic backscatter in the Baltic, North, and Black Seas (Didrikas and Hansson, 2004; Fässler and Gorska, 2009; Marinova and Panayotova, 2015; Panayotova et al., 2014). However, the relative frequency response and the broadband backscatter of sprat in the Mediterranean Sea remain uninvestigated. Only one study, which was conducted in 1994, has been undertaken on the TS of sprat (Azzali et al., 1997), which was recently revised through an *in situ* experiment (Palermo et al., 2023a).

In the present study, we applied an FEM, a BEM, and a KRM model based on detailed sprat swim bladder morphologies obtained through CT scans. The empirical results obtained during the *in situ* experiment presented in Palermo et al. (2023a), which characterized the backscatter of sprat in the Mediterranean Sea, were used to validate model outcomes. We investigated TS as a function of tilt angle, frequency, and fish length to provide the necessary tools for the identification and assessment of the species during dedicated acoustic surveys. We computed the relative frequency response, broadband TS pattern, and the theoretical conversion parameter b_{20} .

2. Materials and methods

2.1. Data collection and image processing

A total of 45 sprat specimens (total length range of 75–119 mm, mean 93.3, s.d. 27 mm) were collected during the MEDIAS 2021 conducted in June and July by the Italian National Research Council - Institute for Marine Biological Resources and Biotechnology (CNR-IRBIM) of Ancona, Italy, on the western side of the Adriatic Sea on board the R/V G. Dallaporta (Leonori et al., 2012). The fishing operations utilized a four-seam pelagic mid-water trawl net with an 18 mm cod-end mesh size, equipped with SIMRAD's FX80 trawl sonar. The net was towed at a depth of approximately 36 m at a speed of around 4 knots for ~30 min. Once on board, active and healthy fish were immediately frozen separately in small boxes for subsequent analysis to prevent any damage to the swim bladder caused by handling duration.

All retained fish were thawed and scanned with a Philips Brilliance 16 P CT at the veterinary facilities of JesiVet in Jesi (AN), Italy (Fig. 1). The optimal settings for the CT scan (Table 1) were obtained from prior trials with several fish of the same dimensions. In each session, 15 specimens were scanned along the transverse axis, obtaining a series of cross-sectional slices. After each session, the total length (TL) and weight of the fish were recorded. DICOM images were imported into 3D Slicer (v. 5.2.1) (Fedorov et al., 2012). The auto-segmentation function in the segment editor was utilized to extract swim bladder shapes by adjusting



Fig. 1. TAC Philips Brilliance 16 P used for sprat scanning at JesiVet, Jesi (AN), Italy.

Table 1
Philips brilliance 16 P computer tomography settings.

CT parameters	Value
Slice thickness (mm)	1.25
Interslice spacing (mm)	0.65
Peak of voltage (KVp)	120
Tube current (mA)	105
Diameter (mm)	430
Exposure time (ms)	350
Filter type	B

the threshold. The resulting 3D model was inspected visually to check for any possible errors and to adjust the boundaries where necessary. Finally, a three-dimensional stereolithography (STL) file was generated and imported into Gmsh software (v. 4.8.4) (Geuzaine and Remacle, 2009). The swim bladder meshes were centered at the origin and scaled to the desired mesh resolution. The main morphological metrics of each swimbladder were extracted (length, height, width, and inclination relative to fish axis).

2.2. Backscatter modeling

FEM, BEM, and KRM models were selected to account for the possible influence of the choice of the model on backscattering results and to compare approximations with numerical models. The selection of two numerical models enabled us to verify the consistency of the computations, which are particularly expensive in terms of time and computational power, compared to approximation models.

The BEM model directly solves the Helmholtz equation by discretizing the boundaries and only dividing the domain's bounding surface, while the FEM model solves the inhomogeneous Helmholtz equation and necessitates the discretization of the entire domain (volume) with the application of a Perfect Matched Layer (PML) (Gonzalez et al., 2020). Nevertheless, we encountered more computational issues in solving the BEM model, mainly due to constraints in available computer memory; therefore, we subsequently employed the FEM model as the reference model.

2.2.1. Finite element method

The STL files from Gmsh were imported into COMSOL Multiphysics (v. 6) (COMSOL, 2021) to apply the numerical Finite Element Method model. In the geometry section, a water sphere was constructed to obtain a water domain of no less than a quarter of the wavelength at each frequency (Ivansson, 2017), surrounded by a PML with a thickness of one-eighth of the wavelength. PML constrains the computational domain in both the temporal and frequency domains. The gas domain (swim bladder geometry), water domain, and PML were meshed with a

resolution of no fewer than 10 mesh elements per wavelength at the highest frequency of 200 kHz. The PML serves as the absorbing domain, functioning as a non-reflecting boundary around the computational domain (water) (Ivansson, 2017). All the parameters are listed in Table S1, and the elements of the FEM model are illustrated in Fig. 2 as an example. The Kirchhoff-Helmholtz integral equation was solved in the frequency domain for each small element computing the far-field backscattered pressure, as reported by Ivansson, 2017:

$$P_{ext}(R) = -\frac{1}{4\pi} \int_{S(r)} e^{\frac{ik(rR)}{|R|}} \left(\nabla p(r) - ikp(r) \frac{R}{|R|} \right) \cdot (-n) dS \quad (3)$$

where p (Pa) is the acoustic pressure, R (m) is the distance from the scatter at which the total field backscatter (1 m in this case) is evaluated, S (m^2) is the water domain surface, r (Pa) represents the incident field at a point on surface S , the vector n represents a unit normal vector indicating the direction of the surface into the region bounded by surface S , and the incident pressure amplitude was set at 1 Pa. Once $P_{ext}(R)$ was obtained, the dorsal Target Strength (TS) of individual fish was determined by computing the exterior field calculation in the z-axis direction, with the query point positioned 1 m away from the fish to simulate a near-surface scenario where depth-related influence is negligible. The TS calculation entails quantifying the logarithmic proportion of the incident energy reflected by the target through the following formula:

$$TS = 10 \log_{10} (P_{ext} / P_{inc}) [\text{dB re } 1 \text{ m}^2] \quad (4)$$

where (P_{inc}) is the incident power intensity given by the density of the medium, the speed of sound, and the amplitude of the incident wave.

2.2.2. Boundary element method

BEM solutions were computed using the open-source Julia implementation of the BEM model in accordance with the methods described by Gonzalez et al. (2020) (https://github.com/elavia/coupled_bem_acoustic).

2.2.3. Kirchhoff-ray-mode model

The STL files of the digitalized swim bladder were converted into xyz point cloud coordinates by dividing the swim bladder into finite-length cylinders of 1 mm thickness. The KRM model calculates the backscatter from individual cylinders relative to the incident acoustic wave and the

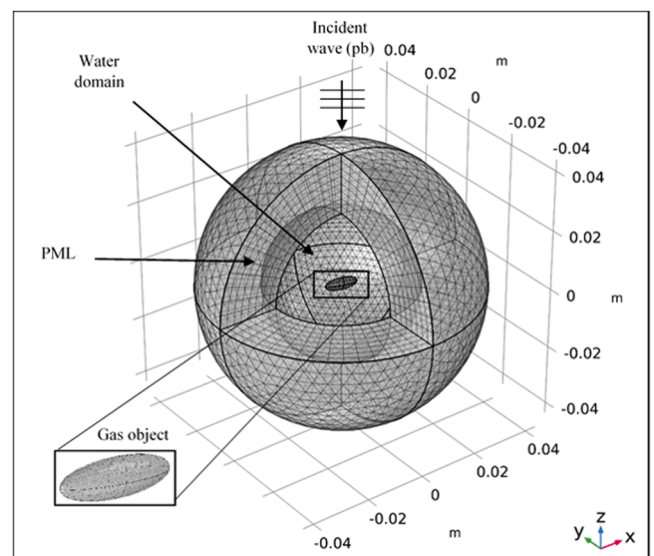


Fig. 2. FEM model showing the geometric scales (x,y,z), the incident background pressure field (pb), and an ellipsoid gas object (dimension: $h = 2$ mm, $l = 6$ mm, $w = 1.3$ mm) simulating a swim bladder in a water domain surrounded by the Perfectly Matched Layer (PML).

carrier frequency, then coherently aggregates the backscatter from each cylinder to determine the overall backscatter from the swim bladder. The KRM model integrates the breathing mode and the Kirchhoff approximation to estimate the intensity of sound reflected by an object (the swim bladder), taking into account the contrasts in sound speed (g) and density (h) associated with the swim bladder (Clay and Horne, 1994). The density and speed of sound values in the swim bladder and water were aligned with those for the FEM model in Table S1.

2.3. *In situ* data

The TS derived from the backscattering models was compared with the results of the empirical experiment described in Palermino et al. (2023a) for the discrete frequencies of 38, 70, 120, and 200 kHz. Following the implementation of a density single target detection algorithm as detailed in Palermino et al. (2023a), the modified Kasatkina method was used to compute the *in situ* TS at frequencies of 38, 70, 120, and 200 kHz. All the *in situ* data originates from two monospecific hauls carried out in the Adriatic Sea.

2.4. Data analysis

TS was computed as a function of acoustic frequency (38–200 kHz, 1 kHz steps), tilt angle ($0^\circ \pm 25^\circ$, 5° steps), and total fish length (L) for single swim bladder 3-D shapes. The TS values were subsequently converted to linear units to compute the average and confidence interval (CI) by tilt angles in the linear domain. The tilt angle range and steps were defined as a trade-off between the computational time required for numerical models, the constraints of the KRM model (acceptable tilt of $\pm 25^\circ$) (Macaulay et al., 2013), and the realistically expected orientation angles in the field (Peña and Foote, 2008; Madirolas et al., 2017). A root mean square error (RMSE) was used to quantify the differences in broadband patterns between backscattering models. The differences between models and *in situ* TS at discrete frequencies were assessed. The relative frequency response using 38 kHz as the reference frequency was computed in the linear domain according to the formula $r_i(f) = \sigma_i(f)/\sigma_i(38)$ (Pedersen et al., 2004). A tilt-averaged TS was estimated from a normal tilt distribution by randomly sampling 500 tilt angles with replacement, spanning from 0 to -25° at 5° intervals, while considering the tilt angle variability of the fish during swimming behavior as the vessel approached. Finally, we computed the standard TS-L model. A 5000 Monte Carlo simulation with random sampling was conducted on the FEM model results to assess the effect of sample size on backscatter estimates of TS at frequencies of 38, 70, 120, and 200 kHz.

3. Results

A total of 45 sprat were scanned; however, only 11 fish presented intact swim bladders deemed suitable for the TS modelling. In the

remaining 34 specimens, there was evidence of outline rupture and partially or fully deflated swim bladders, possibly caused by fishing operations, handling, or preparation processes. The higher frequencies revealed more uncertainty with small sample size being more sensible compared to lower frequencies as shown in Fig. S1. A decrease in uncertainty, as assessed through the Monte Carlo simulation, was detected when increasing from 5 to 10 samples (Fig. S1 and Table S2). TL ranged between 75 and 116 mm, typical for the Adriatic Sea in June/July. TS generally decreased with increasing frequency: at 38, 70, 120 and 200 kHz TS mean = -49.6, -51.5, -54.7 dB re $1 \text{ m}^2 \text{ kHz}$ respectively. Table S3 summarizes the single specimen TL and acoustic backscatter at frequencies of 38, 70, 120, and 200 kHz from the FEM model at the broadside angle (0°). European sprat is characterized by a laterally compressed, ellipsoid, physostomous swim bladder, as shown in Fig. 3 and Fig. S5. Swim bladder dimensions range from 9 to 28 mm in length, 2.2–9.1 mm in height, and 1.8–3.2 m in width, as shown in Table S4. The inclination of the swimbladder relative to the fish axis resulted in two distinct groups: four specimens with a swimbladder tilt between 2.4 and 4° and a second group (7 specimens) ranging from 10 to 19° . The individual specimens' backscatter at broadside incidence, shown in Fig. 4, exhibit three main TS patterns along the simulated frequency range: an almost flat line (e.g., ID 31 and 32), a drop between 70 and 120 kHz followed by an increase up to 200 kHz (e.g., ID 33 and 42), and a constantly decreasing line from 38 kHz to 200 kHz (e.g., ID 46 and 76). In most of the cases, the modeled acoustic backscatter was stronger at 38 and 70 kHz compared to higher frequencies across all models. This is expected for swim bladdered fish, which exhibit a drop in TS between 70 and 120 kHz, followed by a highly shape-dependent, slight increase up to 200 kHz (Fig. 4).

3.1. Scattering comparisons

We observed a strong concordance between *in situ* measurements and the three backscattering models. The mean and CI of TS values from the 11 modeled sprats fall into the 25th and 75th percentiles of the *in situ* TS at 38, 70, and 120 kHz in a tilt angle interval of between 0 and -20° (Fig. 5). The concordance between modeled and measured TS was higher for negative tilt angles than for positive tilt angles (Fig. 5). This may suggest a slight downward escape response by sprat during the *in situ* experiments, a behavior already registered in clupeid species (De Robertis and Handegard, 2013). The discrepancy between the mean *in situ* TS measurements and the two numerical model simulations ranged from 0.1 to -4.4 dB, 0.05 to -9.8 dB, 0.2 to -9.7 dB, and -4.8 to -16.7 dB at frequencies of 38, 70, 120, and 200 kHz, respectively. In contrast, the difference between the mean *in situ* TS and KRM model predictions varied from -1.4 to -6.3 dB at 38 kHz, 0.6 to -9.2 dB at 70 kHz, 0.2 to -10.3 dB at 120 kHz, and -2.9 to -16.6 dB at 200 kHz. Summary statistics of modelled and *in situ* data are provided in Table 2.

A good match between the two numerical models was registered

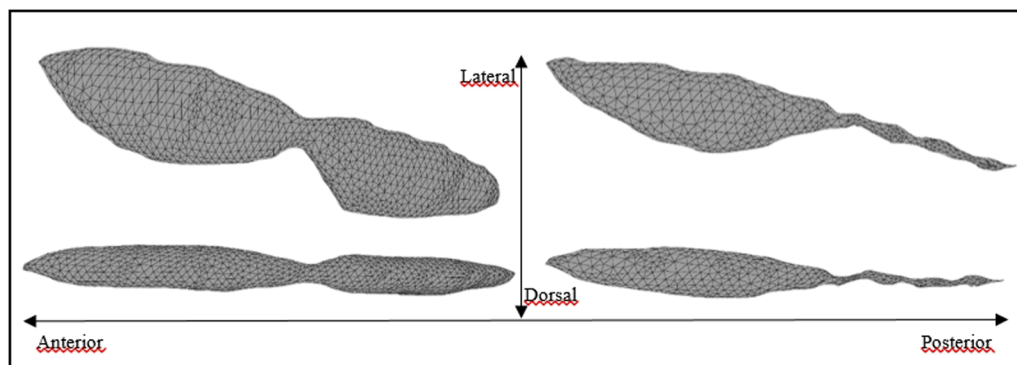


Fig. 3. Examples of sprat swim bladder shape and morphology obtained through computer tomography imaging measurements from lateral (bottom) and dorsal (top) perspectives.

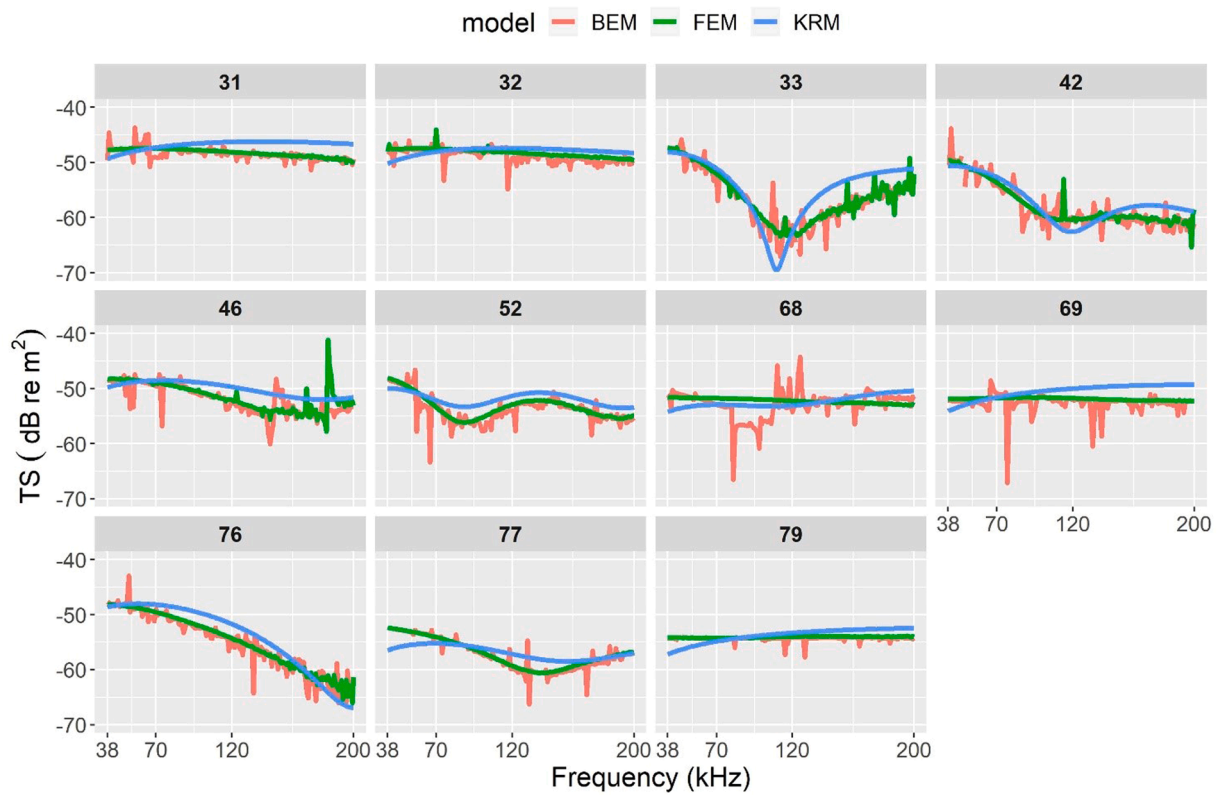


Fig. 4. Single specimens' broadband curve TS at a broadside angle (0°) through backscatter models.

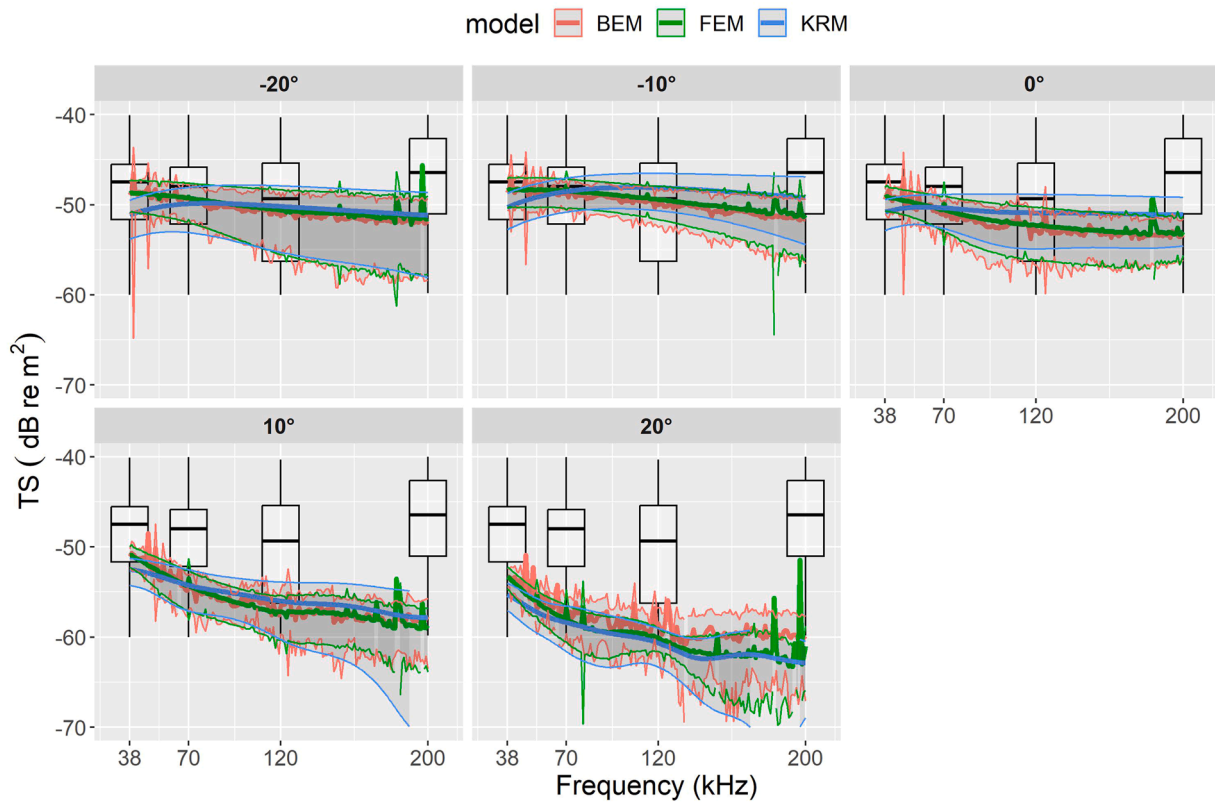


Fig. 5. Mean (solid lines) and 95 % confidence interval (shaded area) of simulated TS from all specimens by tilt angles and backscatter models. The distribution of *in situ* TS at discrete frequencies (38, 70, 120, and 200 kHz) is illustrated in a boxplot, which displays the medians (horizontal lines) and percentiles (box borders and vertical lines).

Table 2
Summary statistics of TS from the entire modeled samples of swim bladders and the in situ dataset.

Frequency (kHz)	Tilt angle (°)	In situ mean TS [25–75 percentile]	FEM mean TS [CI]	BEM mean TS [CI]	KRM mean TS [CI]
38	-20	-48.95	-48.77	-48.38	-51.16
		[-51.62; -45.49]	[-50.87; -47.37]	[-50.41; -47.01]	[-53.83; -49.52]
	-10		-48.45	-48.09	-50.31
			[-50.37; -47.13]	[-49.83; -46.85]	[-52.75; -48.76]
	0		-49.22	-48.92	-50.81
			[-50.76; -48.09]	[-50.20; -47.93]	[-52.86; -49.42]
	10		-50.93	-50.73	-52.53
			[-52.23; -49.93]	[-51.80; -49.88]	[-54.30; -51.28]
	20		-53.28	-53.28	-55.28
			[-54.63; -52.25]	[-54.72; -52.19]	[-57.04; -54.03]
70	-20	-49.18	-49.13	-48.77	-49.90
		[-52.07; -45.75]	[-51.63; -47.56]	[-51.41; -47.14]	[-53.10; -48.08]
	-10		-47.88	-48.01	-48.53
			[-50.56; -46.24]	[-49.42; -46.95]	[-50.82; -47.04]
	0		-49.71	-50.44	-50.36
			[-54.45; -47.50]	[-52.71; -48.95]	[-52.65; -48.88]
	10		-53.50	-54.62	-54.24
			[-58.09; -51.31]	[-58.05; -52.73]	[-57.10; -52.53]
	20		-56.73	-58.00	-58.38
			[-60.53; -54.73]	[-61.29; -56.15]	[-61.62; -56.55]
120	-20	-50.40	-50.60	-50.72	-50.19
		[-56.24; -45.38]	[-55.56; -48.34]	[-55.73; -48.46]	[-55.27; -47.91]
	-10		-49.43	-49.37	-48.13
			[-51.65; -47.96]	[-51.53; -47.94]	[-50.67; -46.53]
	0		-52.28	-52.35	-50.91
			[-56.08; -50.28]	[-56.74; -50.21]	[-54.91; -48.86]
	10		-57.16	-56.63	-56.00
			[-60.29; -55.36]	[-60.76; -54.55]	[-60.25; -53.90]
	20		-60.08	-59.29	-60.66
			[-61.57; -58.97]	[-62.46; -57.48]	[-63.30; -59.03]
200	-20	-46.26	-51.50	-51.29	-51.18
		[-49.85; -41.26]	[-57.71; -49.04]	[-59.81; -48.60]	[-58.07; -48.64]
	-10		-51.13	-51.06	-49.22
			[-55.90; -48.91]	[-56.90; -46.92]	[-54.41; -46.92]
	0		-52.95	-52.91	-51.09
			[-55.61; -51.31]	[-56.46; -50.99]	[-54.57; -49.19]
	10		-59.06	-58.91	-57.82
			[-63.86; -56.84]	[-64.82; -55.90]	[-70.16; -54.94]
	20		-61.00	-62.92	-62.89
			[-65.91; -58.75]	[-66.54; -60.98]	[-68.95; -60.45]

through the RMSE, which measures the overall difference between the broadband curve (RMSE 0° = 2.3 dB; RMSE -10° = 2.5 dB; RMSE -20° = 4 dB). However, the difference rises with an increasing tilt angle (RMSE 10° = 5.9 dB; RMSE 20° = 5.1 dB), as shown in Fig. 5. This difference may be due to a few more glitches detected in the BEM model, caused by possible numerical issues during computations or due to the limited RAM and CPU available during the computation (see Fig. S3). The KRM exhibits greater divergence from the FEM model at broadside and higher tilt angles (RMSE 0° = 3.5 dB; RMSE -10° = 4.8 dB; RMSE

-20° = 5.6 dB; RMSE 10° = 4.7 dB; RMSE 20° = 4.7 dB), while uncertainty rises linearly as frequency increases.

The mean TS computed as a function of frequency and tilt angles showed fewer fluctuations in TS at lower frequencies (Fig. 6). The three backscatter models followed the same general trends, even when considering individual specimens. The KRM generally showed deeper nulls and higher peaks (Figs. S2, S3, and S4). Excluding values with apparent glitches in the BEM and FEM models (see Fig. S3), the TS peaked at a tilt of -15° and a frequency of 70 kHz, yielding TS values of -48.1 and -47.9 dB (dB re 1 m²), respectively. Conversely, with KRM, the maximum TS occurred at a tilt of -10° at frequencies approaching 120 kHz. In general terms, higher TS for all frequencies were observed with negative tilt angles (0 to -25°) while TS decreased with positive tilt angles (Figs. 5 and 6).

3.2. Relative frequency response and TS-L relationship

The FEM model predictions yielded values closest to the *in situ* measurements, with the exception of 200 kHz, and exhibited reduced susceptibility to numerical calculation errors compared to the BEM model. Therefore, the FEM model was deemed the most stable model in our scenarios and used for the computation of the relative frequency response curves and TS-L relationships. Assuming a tilt angle of 10° and 20°, the *ri(f)* settles at a decreasing ratio of ~0.5 at 70 kHz, ~0.2 at 120 kHz, and ~0.2 at 200 kHz. Conversely, at a tilt angle of 0° (broadside angle), -10°, -20°, and tilt averaged, the *ri(f)* is closer to 1, remaining slightly below 1 at 0° and -20° and above 1 at -10° (Fig. 7). Fig. 7 illustrates a general decreasing trend in the relative frequency response from 70 to 200 kHz across all tilt angle intervals. Tilt angle has a strong effect, especially at 38 and 70 kHz.

The FEM-derived TS-L relationship at 38 kHz for the 11 modeled sprat was summarized at a set of different tilt angles (0°, 10°, 20°, and tilt averaged). As expected, a linear increase of TS with L was observed (R² = 0.2; F = 2.7; p ≤ 0.001) (Fig. 8). The values exhibit more dispersion around the slope at lower L (75–86 mm). The *b*_{20s} ranged from -68.5 to -67.9 dB re 1 m², indicating low variability among the assuming tilt angles. At 0°, the standard model produced an *m* of 16.5 and a *b* of -65.2 dB re 1 m². At 10° and 20°, *m* is closer to 20, and *b* is lower relative to 0° (-69.3 and -70.1 dB re 1 m², respectively). For an averaged tilt angle, the standard model yielded almost the same results as the model with the slope forced to 20 (*m* = 20.3, *b* = -68.6).

4. Discussion

Among acoustic scattering models, numerical models such as the BEM and FEM are considered more precise than approximate models such as the KRM (Jech et al., 2015); nonetheless, they are computationally expensive (several hours or days for a single fish using consumer-grade equipment). Consequently, approximation models are often preferred (Yoon et al., 2023; Yang et al., 2023). However, several authors demonstrated their inability to capture finer scale variations that can affect the overall backscatter (Jech et al., 2015; Macaulay et al., 2013), in contrast to numerical models (Boswell et al., 2020). This study revealed minor divergences between numerical models (FEM and BEM) and the approximate analytical KRM model in the broadband pattern of up to 2 dB in mean TS at 38 kHz (RMES ranged from 3.5 to 5.6 dB). Overall, the RMSE values are higher than those reported by Macaulay et al. (2013), who compared KRM and FEM of prolate spheroids with an analytical solution. In this study, we analyzed real, more complex swim bladder shapes that may explain the higher differences between models. We detected higher differences in the broadband frequency response comparison for specimens characterized by shrinkage along the swim bladder profile, such as for specimen ID numbers 33, 46, and 52 (Fig. 4 and S3). Nonetheless, in many cases, the performance of KRM model should be sufficient. This is especially true in scenarios that do not require higher accuracy in detecting minor individual variations in

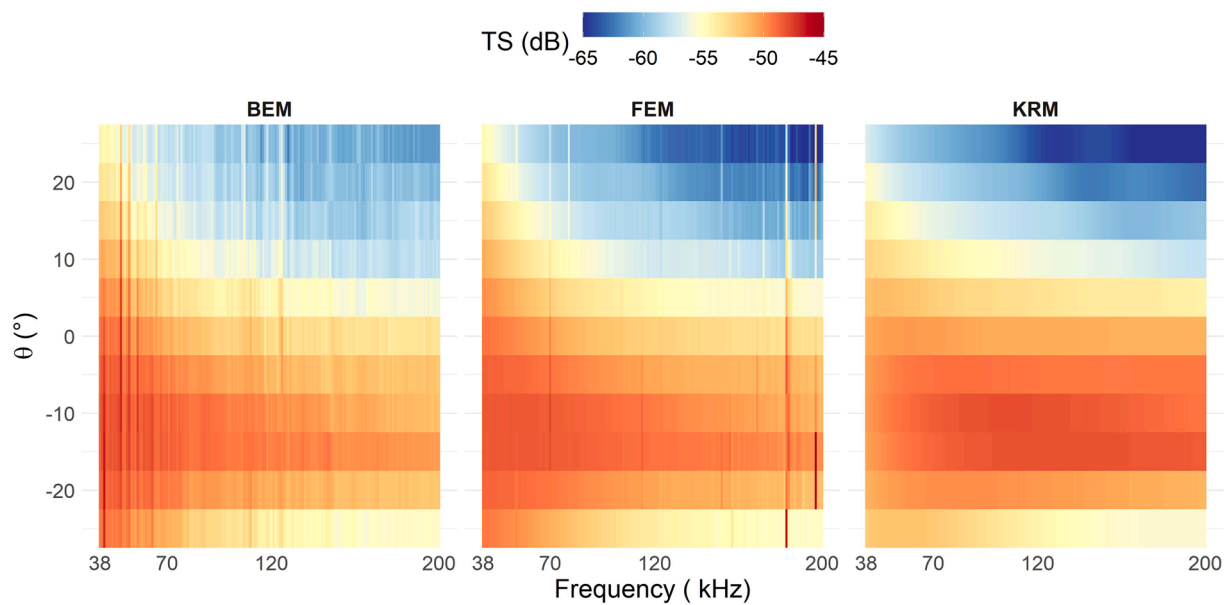


Fig. 6. Simulated mean TS from the entire sprat sample ($n = 11$) as a function of frequency (38–200 kHz) and tilt angle ($\pm 25^\circ$; 5° steps), where 0° represents the broadside angle.

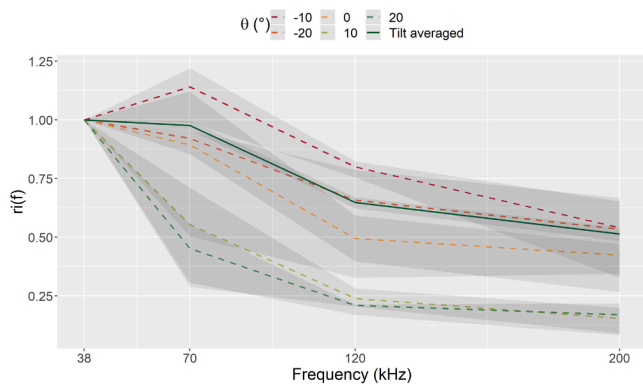


Fig. 7. Mean relative frequency responses of sprat (continuous line) and confidence intervals (dashed area) at different tilt angles.

acoustic backscatter owing to the target's morphological characteristics. The glitches identified during FEM computations are mostly due to complications in solving the Kirchhoff-Helmholtz integral equation at higher frequencies for IDs 46 and 33 in COMSOL software (Fig. S4). A higher order of elements can yield more accurate results but may increase computational complexity, especially for the finer swim bladder portions. Setting the same mesh size in both the BEM and FEM models may have affected the numerical stability and convergence properties of the BEM model, which typically requires a finer mesh for the boundaries, resulting in the glitches presented in Fig. S3 (Gonzalez et al., 2020). The BEM model may perform better for lower frequency ranges and simpler geometries, whereas the FEM may be more robust for higher frequencies and more complex structures. However, FEM models may exhibit diminished accuracy for weaker scatterers (with an acoustic impedance close to the ambient water) (Jech et al., 2015). We detected an increasing difference in TS with rising tilt angle and frequency, resulting in reduced TS attributed to the smaller size of the swim bladder cross-section. Overall, the FEM model produced more stable estimates, especially at lower frequencies. Utilizing the BEM solution as a benchmark in accordance with Jech et al. (2015), we assert that the FEM model enhances the detection of small variations in the swim bladder shape, despite the irregularities found during the computation (see

Fig. 4 and S4).

Our findings revealed individual heterogeneity and high bias attributable to the tilt angle of the fish in broadband TS patterns. This is in agreement with previous studies on *Engraulidae* species (Madirolas et al., 2017; Sobradillo et al., 2021). Model results can be useful to interpret the tilt angle displacement of the fish during *in situ* measurements. Taking the backscattering models as a reference point, we can estimate the tilt angle of individual fish during the *in situ* measurements ranged between 0 and -20° (Palermo et al., 2023a).

The broadband backscatter by tilt angles presented in Figs. 5 and 6 represents one of the first broadband acoustic studies conducted in the Mediterranean Sea (Palermo et al., 2023b). Overall, TS demonstrated greater stability at around 38 kHz, with variability increasing with tilt angles and frequency. This renders 38 kHz the most suitable frequency for abundance or biomass estimates in routine sprat fisheries acoustics surveys. The broadband TS values obtained in this study are lower than those estimated for the North Sea by Antona (2016). The size of the fish may have caused these differences since, the aforementioned work, analysed fish considerably longer than our specimens. Antona (2016) measured the flesh density of sprat by calculating the sound speed within the fish body, a factor not addressed in the present study. Moreover, TS may differ across areas, as reported for herring and other species (Ganias et al., 2015; Ok and Gücü, 2019; Ona, 1990), since the physical environment may influence fish physiology and morphology, leading to morphological variations attributable to differences in life history traits (Scoles and Graves, 1988). The overall spectra presented in Fig. 5 diverge from the findings of Antona (2016), who detected a null at 90 kHz and higher TS values at 200 kHz relative to 38 kHz. In the current investigation, an increase in mean TS was observed from *in situ* experiment computations between 120 and 200 kHz, with higher values at 200 kHz than at 38 kHz. A rising TS from 120 to 200 kHz was identified for several specimens computed by means of the FEM model (Fig. 4). In all cases, TS values at 38 kHz were higher or equivalent to those at 200 kHz. Antona (2016) included the contribution of backbones in the computation of fish total backscatter that have not been considered in the present study due to available computational power and time constraints. Backbones backscatter may have implications on TS especially at higher frequencies and may have caused a shadowing effect at low tilt angles during the *in situ* experiment described in Palermo et al. (2023a), which would explain the discrepancies found in this work at

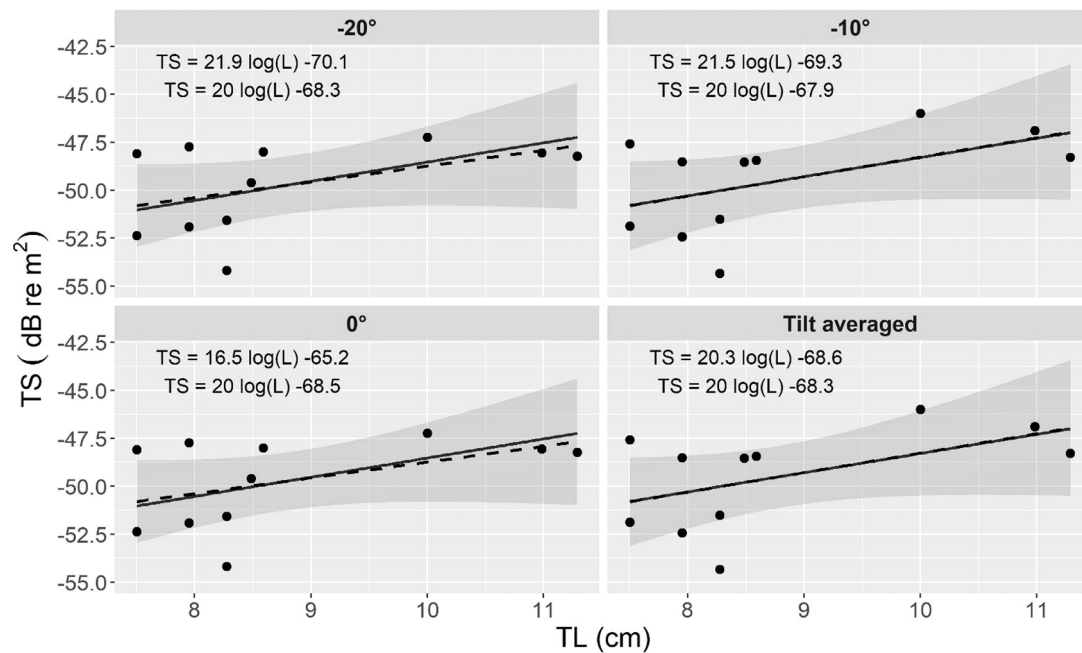


Fig. 8. FEM model TS vs. TL relationships at 38 kHz by different tilt angles. The standard model regression is represented by a dashed line, while the continuous line indicates the model with the slope forced to 20. Both equations are reported in the top left corner of each plot. The dashed area represents the 95 % confidence interval.

200 kHz between models and empirical results (Pérez-Arjona et al., 2020).

The present work demonstrated the variability of $ri(f)$ due to the tilt angle of sprat specimens. Considering a tilt angle average, $ri(f)$ is comparable with the *in situ* measurements. Our findings, albeit based on models, may be useful to differentiate between the three main clupeid and engraulidae species that inhabit the Mediterranean Sea: *Sardina pilchardus*, *Engraulis encrasicolus*, and *Sprattus sprattus*. The three species exhibit the typical trend of swim bladdered pelagic fish, marked by a sharp decrease in TS from lower to higher frequencies, making them suitable for assessment at 38 kHz. Sardine presents a high ratio between 38 and 120 kHz, with a drop up to 0.4 $ri(f)$ at 200 kHz, while anchovy is characterized by a sharp decrease in ratio up to 120 kHz, followed by a stable trend at 200 kHz (De Felice et al., 2015; Fernandes et al., 2005). The relative frequency response of sprat is positioned between that of anchovy and sardine. It is characterized by a relatively high ratio between 38 and 120 kHz (0.70) and a quite similar ratio between 120 and 200 kHz.

This study investigated the TS-L relationship as a function of tilt angle, finding different b and b_{20} values. Generally, the estimated slopes resulted in m values close to 20, suggesting an isometric growth of the swim bladder in relation to fish size, in agreement with the model proposed by Foote in 1987 for clupeid species. Assuming the tilt-averaged TS as the more reasonable assumption for swimming fish, we proposed a conversion factor b_{20} for sprat of -68.35 dB re 1 m^2 . The regressions depicted in Fig. 8 highlight a spread of TS values at the small sizes, which could be attributable to specimens collected in different hauls. Notably, within the size range of 75–90 mm, the four values above the regression lines correspond to specimens obtained from the same haul, whereas the four values below the regression lines are from a different haul. The specimens were captured in hauls characterized by a slight difference in depth (35 and 27 m) and different times of the day (one in the morning and the other in the evening). Therefore, the difference in TS of up to 5 dB within the size range of 75–90 cm, presented in Table S3, may be due to different inflations of the swim bladder which may be attributed to behavioral differences among the fish and changes in ambient pressure, leading to an adjustment in the swim bladder's

inflation rate.

The dearth of *in situ* and *ex situ* experiments on European sprat in the Mediterranean Sea for biomass estimates underlines the importance of using the backscattering models (Azzali et al., 1997; Palermino et al., 2023a). The comparison between the new model-based b_{20} value found herein and the one in use in the Adriatic Sea ($b_{20} = -71.7$ dB re 1 m^2) and Mediterranean Sea yields a difference of ~ 3.2 dB (De Felice et al., 2021). This translates into more than a two-fold decrease in the linear space, potentially leading to a 25 % reduction in biomass (Palermino et al., 2023a). Nevertheless, all the model-based b_{20} provided in this work were within the range of -67.5 and -68.8 dB re 1 m^2 , as proposed by Palermino et al. (2023a). The small sample size and the post-capture handling process of the fish may have biased our results. However, the sensitivity analysis conducted through the 5000 Monte Carlo simulation demonstrated that the increase in sample size would have exerted a minimal impact on the backscatter uncertainty and mean values. Moreover, backscattering model studies rarely involve a large number of specimens (Boswell et al., 2020; Ok and Gücü, 2019; Yang et al., 2023). All the retained fish had intact and quite regular swim bladder profiles, despite a high variability in shape. The results presented in Fig. 5 and Fig. 8 show a general decreasing trend with increasing frequency and an increase in TS with size, as expected for swim bladdered fish. The presented agreement between the modeled and empirical data gives robustness to both analyses, which provided a b_{20} value that may be particularly valuable for biomass assessment purposes.

5. Conclusions

This study presents, for the first time, the relative frequency response and broadband backscatter of European sprat in the Mediterranean Sea. The results produced can be implemented in acoustic post-processing analysis to estimate abundance or biomass or as a diagnostic tool for accurate species identification. Our conversion parameter aligns with empirical estimates and may serve as the new reference value for sprat in the Mediterranean Sea. However, a greater supply of monospecific hauls is still needed to incorporate it into the quantitative evaluation process. The objective of backscattering models is not to supplant empirical

measurements. Rather, due to the dearth of empirical data, they are valuable for filling information gaps regarding species that do not easily fit the requirements for the *in situ* method and in validating target strength trials. One such example is sprat in the Mediterranean Sea. The integration of a backscattering model has contributed crucial information to our understanding of the acoustic reflectivity of sprat in this region. Accordingly, additional efforts should be undertaken to increase the amount of *in situ* measurements Korneliusen collected using wide-band split-beam transducers.

CRedit authorship contribution statement

Palermino Antonio: Writing – original draft, Visualization, Methodology, Formal analysis, Conceptualization. **Gastauer Sven:** Writing – review & editing, Methodology, Formal analysis, Conceptualization. **De Felice Andrea:** Writing – review & editing, Validation, Supervision. **Canduci Giovanni:** Writing – review & editing, Investigation. **Biagiotti Ilaria:** Writing – review & editing, Investigation. **Leonori Iole:** Writing – review & editing, Validation, Supervision, Resources.

Declaration of Competing Interest

The authors declare that they have no known competing financial interests or personal relationships that could have appeared to influence the work reported in this paper.

Acknowledgment

The research work that led to these results was carried out in the framework of the PhD project “Innovative Technologies and Sustainable Use of Mediterranean Sea Fishery and Biological Resources” (FishMed-PhD). The study was largely supported by the MEDIAS research project within the framework of the EC-MIPAAF Italian National Fisheries Data Collection Programs. The authors express their gratitude to the captain and crew of the R/V Dallaporta, as well as the researchers and technical personnel involved in the scientific surveys. Special thanks are due to the technicians Giordano Giuliani and Giuseppe Caccamo for their help in gathering data. The authors would like to thank the JesiVet veterinary clinic for making the computer tomography scans possible and for helping with them. Our sincere gratitude to the colleagues at the Institute of Marine Research of Bergen, Norway, for their valuable advice. We are grateful to Eurostreet for the language revision.

Appendix A. Supporting information

Supplementary data associated with this article can be found in the online version at [doi:10.1016/j.fishres.2025.107298](https://doi.org/10.1016/j.fishres.2025.107298).

Data availability

Data will be made available on request.

References

- Anderson, V.C., 1950. Sound scattering from a fluid sphere. *J. Acoust. Soc. Am.* 22, 426–431. <https://doi.org/10.1121/1.1906621>.
- Antona, A., 2016. Remote Fish Species and Size Identification Using Broadband Echosounders.
- Ayoubi, S., El, Mamza, K., Fujino, T., Abe, K., Amakasu, K., Miyashita, K., 2016. Estimation of target strength of *Sardina pilchardus* and *Sardinella aurita* by theoretical approach. *Fish. Sci.* 82, 417–423. <https://doi.org/10.1007/s12562-016-0986-8>.
- Azzali, M., Cosimi, G., Luna, M., 1997. La biomassa, la struttura delle aggregazioni e la distribuzione geografica delle popolazioni di acciughe e sardine nel Basso Adriatico, stimate con la metodologia acustica.
- Bairstow, F., Gastauer, S., Wotherspoon, S., Brown, C.T.A., Kawaguchi, S., Edwards, T., Cox, M.J., 2022. Krill biomass estimation: sampling and measurement variability. *Front. Mar. Sci.* 9, 1–19. <https://doi.org/10.3389/fmars.2022.903035>.
- Bassett, C., Robertis, A.De, Wilson, C.D., 2018. Broadband echosounder measurements of the frequency response of fishes and euphausiids in the Gulf of Alaska. *ICES J. Mar. Sci.* 75, 1131–1142. <https://doi.org/10.1093/icesjms/fsx204>.
- Benoit-Bird, K.J., Waluk, C.M., 2020. Exploring the promise of broadband fisheries echosounders for species discrimination with quantitative assessment of data processing effects. *J. Acoust. Soc. Am.* 147, 411–427. <https://doi.org/10.1121/10.0000594>.
- Boswell, K.M., Pedersen, G., Taylor, J.C., Labua, S., Patterson, W.F., 2020. Examining the relationship between morphological variation and modeled broadband scattering responses of reef-associated fishes from the Southeast United States. *Fish. Res.* 228, 105590. <https://doi.org/10.1016/j.fishres.2020.105590>.
- Clay, C.S., Horne, J.K., 1994. Acoustic models and target strengths of the Atlantic cod (*Gadus morhua*). *J. Acoust. Soc. Am.* 96, 2350–2351. <https://doi.org/10.1121/1.404903>.
- COMSOL, 2021. COMSOL Multiphysics® v. 6.2 [WWW Document]. COMSOL AB, Stockholm, Sweden.
- De Felice, A., Canduci, G., Biagiotti, I., Costantini, I., Leonori, I., 2015. Small Pelagics Multifrequency Fingerprints in the Adriatic Sea. <https://doi.org/10.13140/RG.2.2.33006.61764>.
- De Felice, A., Iglesias, M., Sarau, C., Bonanno, A., Ticina, V., Leonori, I., Ventero, A., Hattab, T., Barra, M., Gasparevic, D., Biagiotti, I., Bourdeix, J.-H., Genovese, S., Juretic, T., Aronica, S., Malavolti, S., 2021. Environmental drivers influencing the abundance of round sardinella (*Sardinella aurita*) and European sprat (*Sprattus sprattus*) in different areas of the Mediterranean Sea. *Mediterr. Mar. Sci.* 22, 812–826. <https://doi.org/10.12681/mms.25933>.
- De Robertis, A., Handegard, N.O., 2013. Fish avoidance of research vessels and the efficacy of noise-reduced vessels: a review. *ICES J. Mar. Sci.* 70, 34–45. <https://doi.org/10.1093/icesjms/fss155>.
- Didrikas, T., Hansson, S., 2004. In situ target strength of the Baltic Sea herring and sprat. *ICES J. Mar. Sci.* 61, 378–382. <https://doi.org/10.1016/j.icesjms.2003.08.003>.
- Fanelli, E., Da Ros, Z., Menicucci, S., Malavolti, S., Biagiotti, I., Canduci, G., De Felice, A., Leonori, I., 2023. The pelagic food web of the Western Adriatic Sea: a focus on the role of small pelagics. *Sci. Rep.* 13, 14554. <https://doi.org/10.1038/s41598-023-40665-w>.
- FAO, 2023. The State of Mediterranean and Black Sea Fisheries 2023 - Special Edition, General Fisheries Commission for the Mediterranean. FAO, Rome. <https://doi.org/10.4060/cc3370en>.
- Fässler, S.M.M., Gorska, N., 2009. On the target strength of Baltic clupeids. *ICES J. Mar. Sci.* 66, 1184–1190. <https://doi.org/10.1093/icesjms/fsp005>.
- Fässler, S.M.M., O'Donnell, C., Jech, J.M., 2013. Boarfish (*Capros aper*) target strength modelled from magnetic resonance imaging (MRI) scans of its swimbladder. *ICES J. Mar. Sci.* 70, 1451–1459. <https://doi.org/10.1093/icesjms/fst095>.
- Fedorov, A., Beichel, R., Kalpathy-Cramer, J., Finet, J., Fillion-Robin, J.C., Pujol, S., Bauer, C., Jennings, D., Fennessy, F., Sonka, M., Buatti, J., Aylward, S., Miller, J.V., Pieper, S., Kikinis, R., 2012. 3D Slicer as an image computing platform for the Quantitative Imaging Network. *Magn. Reson. Imaging* 30, 1323–1341. <https://doi.org/10.1016/j.mri.2012.05.001>.
- Fernades et al., 2005. The SIMFAMI project: Species Identification Methods From Acoustic Multi-frequency Information, Final Report to the EC Number Q5RS-2001-02054.
- Foote, G., 1980. Importance of the swimbladder in acoustic scattering by fish: A comparison of gadoid and mackerel target strengths. *J. Acoust. Soc. Am.* 67, 2084–2089.
- Foote, K.G., 1987. Fish target strengths for use in echo integrator surveys. *J. Acoust. Soc. Am.* 82, 981–987. <https://doi.org/10.1121/1.395298>.
- Francis, D.T.I., Foote, K.G., 2003. Depth-dependent target strengths of gadoids by the boundary-element method. *J. Acoust. Soc. Am.* 114, 3136–3146. <https://doi.org/10.1121/1.1619982>.
- Furusawa, M., 1988. Prolate spheroidal models for predicting general trends of fish target strength. *J. Acoust. Soc. Jpn.* 9, 13–24.
- Ganias, K., Michou, S., Nunes, C., 2015. A field based study of swimbladder adjustment in a physostomous teleost fish. *PeerJ* 3, 892. <https://doi.org/10.7717/peerj.892>.
- Gastauer, S., Scoulding, B., Parsons, M., 2017. Estimates of variability of goldband snapper target strength and biomass in three fishing regions within the Northern Demersal Scalefish Fishery (Western Australia). *Fish. Res.* 193, 250–262. <https://doi.org/10.1016/j.fishres.2017.05.001>.
- Gastauer, S., Scoulding, B., Fässler, S.M.M., Benden, D.P.L.D., Parsons, M., 2016. Target strength estimates of red emperor (*Lutjanus sebae*) with Bayesian parameter calibration. *Aquat. Living Resour.* 29, 301. <https://doi.org/10.1051/alr/2016024>.
- Geuzaine, C., Remacle, J.F., 2009. Gmsh: A 3-D finite element mesh generator with built-in pre- and post-processing facilities. *Int. J. Numer. Methods Eng.* 79, 1309–1331. <https://doi.org/10.1002/nme.2579>.
- Gonzalez, J.D., Lavia, E.F., Blanc, S., Maas, M., Madirolas, A., 2020. Boundary element method to analyze acoustic scattering from a coupled swimbladder-fish body configuration. *J. Sound Vib.* 486, 115609. <https://doi.org/10.1016/j.jsv.2020.115609>.
- Gorska, N., Ona, E., 2003. Modelling the acoustic effect of swimbladder compression in herring. *ICES J. Mar. Sci.* 60, 548–554. <https://doi.org/10.1016/S1054>.
- Gugele, S.M., Widmer, M., Baer, J., DeWeber, J.T., Balk, H., Brinker, A., 2021. Differentiation of two swim bladdered fish species using next generation wideband hydroacoustics. *Sci. Rep.* 11, 1–10. <https://doi.org/10.1038/s41598-021-89941-7>.
- Hazen, E.L., Horne, J.K., 2004. Comparing the modelled and measured target-strength variability of walleye pollock, *Theragra chalcogramma*. *ICES J. Mar. Sci.* 61, 363–377. <https://doi.org/10.1016/j.icesjms.2004.01.005>.

- Horne, J., 2000. Comparing acoustic model predictions to in situ backscatter measurements of fish with dual-chambered swimbladders. *J. Fish. Biol.* 57, 1105–1121. <https://doi.org/10.1006/jfbi.2000.1372>.
- Ivansson, S., 2017. Sound propagation modeling. In: *Applied Underwater Acoustics*. Elsevier, pp. 185–272. <https://doi.org/10.1016/B978-0-12-811240-3.00003-5>.
- Jech, J.M., Horne, J.K., Chu, D., Demer, D.A., Francis, D.T.I., Gorska, N., Jones, B., Lavery, A.C., Stanton, T.K., Macaulay, G.J., Reeder, D.B., Sawada, K., 2015. Comparisons among ten models of acoustic backscattering used in aquatic ecosystem research. *J. Acoust. Soc. Am.* 138, 3742–3764. <https://doi.org/10.1121/1.4937607>.
- Jech, J.M., Schael, D.M., Clay, C.S., 1995. Application of three sound scattering models to threadfin shad (*Dorosoma petenense*). *J. Acoust. Soc. Am.* 98, 2262–2269. <https://doi.org/10.1121/1.413340>.
- Korneliussen, R.J., 2018. Acoustic target classification. *ICES Coop. Res. Rep.* No 344. <https://doi.org/10.17895/ices.pub.4567>.
- Korneliussen, R.J., Ona, E., 2002. An operational system for processing and visualizing multi-frequency acoustic data. *ICES J. Mar. Sci.* 59, 293–313. <https://doi.org/10.1006/jmsc.2001.1168>.
- Kubilius, R., Macaulay, G.J., Ona, E., 2020. Remote sizing of fish-like targets using broadband acoustics. *Fish. Res.* 228, 105568. <https://doi.org/10.1016/j.fishres.2020.105568>.
- Lavia, E.F., Gonzalez, J.D., Menna, B.V., Prario, I., Cascallares, G., Cabreira, A.G., Madirolas, A., Blanc, S., 2020. Numerical modelling of broadband acoustic signatures for two Argentinian swimbladdered fish species. In: *2020 IEEE Congreso Bial de Argentina (ARGENCON)*. IEEE, pp. 1–7. <https://doi.org/10.1109/ARGENCON49523.2020.9505349>.
- Leonori, L., Tičina, V., De Felice, A., Vidjak, O., Grubišić, L., Pallaoro, A., 2012. Comparisons of two research vessels' properties in the acoustic surveys of small pelagic fish. *Acta Adriat.* 53 (3), 389–398.
- Leonori, L., Tičina, V., Giannoulaki, M., Hattab, T., Iglesias, M., Bonanno, A., Costantini, I., Canduci, G., Machias, A., Ventero, A., Somarakis, S., Tsagarakis, K., Bogner, D., Barra, M., Basilone, G., Genovese, S., Juretić, T., Gasparević, D., De Felice, A., 2021. History of hydroacoustic surveys on small pelagic fish species in the European Mediterranean Sea. *Med. Mar. Sci.* 22 (4), 751–768. <https://doi.org/10.12681/mms.26001>.
- Macaulay, G.J., Peña, H., Fässler, S.M.M., Pedersen, G., Ona, E., 2013. Accuracy of the Kirchhoff-Approximation and Kirchhoff-Ray-Mode Fish swimbladder acoustic scattering models. *PLoS One* 8, e64055. <https://doi.org/10.1371/journal.pone.0064055>.
- Madirolas, A., Membiola, F.A., Gonzalez, J.D., Cabreira, A.G., Dell'Erba, M., Prario, I.S., Blanc, S., 2017. Acoustic target strength (TS) of argentine anchovy (*Engraulis anchoita*): the nighttime scattering layer. *ICES J. Mar. Sci.* 74, 1408–1420. <https://doi.org/10.1093/icesjms/fsw185>.
- Marinova, V., Panayotova, M., 2015. In situ target strength measurements of sprat (*Sprattus sprattus* L.) in the Western Black Sea. *Comptes Rendus L'Acad. Bulg. Des. Sci.* 68, 1253–1258.
- MEDIAS, 2018. Report of the 11th meeting for Mediterranean International Acoustic Survey (MEDIAS). Steering Committee Report. Ancona, Italy, 17–19 April 2018. 91 pp.
- Membiola, F.A., dell'Erba, M.G., 2018. A hydrodynamic analytical model of fish tilt angle: Implications regarding acoustic target strength modelling. *Ecol. Modell.* 387, 70–82. <https://doi.org/10.1016/j.ecolmodel.2018.05.022>.
- O'Driscoll, R.L., 2004. Estimating uncertainty associated with acoustic surveys of spawning hoki (*Macrurus novaezelandiae*) in Cook Strait, New Zealand. *ICES J. Mar. Sci.* 61, 84–97. <https://doi.org/10.1016/j.icesjms.2003.09.003>.
- O'Driscoll, R.L., Canese, S., Ladroit, Y., Parker, S.J., Ghigliotti, L., Mormede, S., Vacchi, M., 2018. First in situ estimates of acoustic target strength of Antarctic toothfish (*Dissostichus mawsoni*). *Fish. Res.* 206, 79–84. <https://doi.org/10.1016/j.fishres.2018.05.008>.
- O'Driscoll, R.L., Macaulay, G.J., Gauthier, S., Pinkerton, M., Hanchet, S., 2011. Distribution, abundance and acoustic properties of Antarctic silverfish (*Pleuragramma antarcticum*) in the Ross Sea. *Deep Sea Res. Part II Top. Stud. Oceanogr.* 58, 181–195. <https://doi.org/10.1016/j.dsr2.2010.05.018>.
- Ok, M., Gücü, A.C., 2019. A study on European anchovy (*Engraulis encrasicolus*) swimbladder with some considerations on conventionally used target strength. *Turk. J. Zool.* 43, 203–214. <https://doi.org/10.3906/zoo-1809-21>.
- Ona, E., 1990. Physiological factors causing natural variations in acoustic target strength of fish. *J. Mar. Biol. Assoc. U.K.* 70, 107–127. <https://doi.org/10.1017/S002531540003424X>.
- Palermino, A., De Felice, A., Canduci, G., Biagiotti, I., Costantini, I., Centurelli, M., Leonori, L., 2023a. Preliminary target strength measurement of *Sprattus sprattus* and its influence on biomass estimates in the Adriatic Sea (Mediterranean Sea). *Fish. Res.* 266, 106777. <https://doi.org/10.1016/j.fishres.2023.106777>.
- Palermino, A., De Felice, A., Canduci, G., Biagiotti, I., Costantini, I., Centurelli, M., Leonori, L., 2023b. Application of an analytical approach to characterize the target strength of ancillary pelagic fish species. *Sci. Rep.* 13, 15182. <https://doi.org/10.1038/s41598-023-42326-4>.
- Palermino, A., De Felice, A., Canduci, G., Biagiotti, I., Costantini, I., Centurelli, M., Menicucci, S., Gasparević, D., Tičina, V., Leonori, L., 2024. Modeling of the habitat suitability of European sprat (*Sprattus sprattus*, L.) in the Adriatic Sea under several climate change scenarios. *Front. Mar. Sci. Sec. Marine Fisheries, Aquaculture and Living Resources* 11, 1383063. <https://doi.org/10.3389/fmars.2024.1383063>.
- Panayotova, M., Raykov, V.S., Stefanova, K., Krastev, A., 2014. Pilot acoustic study of fish stocks distribution in the Northern Bulgarian Black Sea area. *Comptes Rendus L'Acad. Bulg. Des. Sci.* 67, 959–964.
- Pedersen, G., Korneliussen, R.J., Ona, E., 2004. The Relative Frequency Response, as Derived from Individually Separated Targets on Cod, Saithe and Norway pout by Material & Methods.
- Peña, H., Foote, K.G., 2008. Modelling the target strength of *Trachurus symmetricus murphyi* based on high-resolution swimbladder morphometry using an MRI scanner. *ICES J. Mar. Sci.* 65, 1751–1761. <https://doi.org/10.1093/icesjms/fsn190>.
- Pérez-Arjona, I., Godinho, L., Espinosa, V., 2020. Influence of fish backbone model geometrical features on the numerical target strength of swimbladdered fish. *ICES J. Mar. Sci.* 77, 2870–2881. <https://doi.org/10.1093/icesjms/fsaa160>.
- Reeder, D.B., Jech, J.M., Stanton, T.K., 2004. Broadband acoustic backscatter and high-resolution morphology of fish: measurement and modeling. *J. Acoust. Soc. Am.* 116, 747–761. <https://doi.org/10.1121/1.1648318>.
- Salvetat, J., Lebourges-Dhaussy, A., Travassos, P., Gastauer, S., Roudaut, G., Vargas, G., Bertrand, A., 2020. In situ target strength measurement of the black triggerfish *Melichthys niger* and the ocean triggerfish *Canthidermis sufflamen*. *Mar. Freshw. Res.* 71, 1118–1127. <https://doi.org/10.1071/MF19153>.
- Sawada, K., Furusawa, M., Williamson, N.J., 1993. Conditions for the precise measurement of fish target strength in situ. *J. Mar. Acoust. Soc. Jpn.* 20, 73–79. <https://doi.org/10.3135/jmasj.20.73>.
- Schickele, A., Goberville, E., Leroy, B., Beaugrand, G., Hattab, T., Francour, P., Raybaud, V., 2021. European small pelagic fish distribution under global change scenarios. *Fish. Fish.* 22, 212–225. <https://doi.org/10.1111/faf.12515>.
- Scoles, D., Graves, J.E., 1988. Global phylogeography of mackerels of the genus *Scomber*. *Fish. Bull.* 96, 823–842.
- Scouling, B., Gastauer, S., MacLennan, D.N., Sascha, M.M.F., Copland, P., Fernandes, P. G., 2017. Effects of variable mean target strength on estimates of abundance: the case of Atlantic mackerel (*Scomber scombrus*). *ICES J. Mar. Sci.* 74, 822–831. <https://doi.org/10.1093/icesjms/fsw212>.
- Simmonds, J.E., MacLennan, D.N., 2005. *Fisheries Acoustic: Theory and Practice*. Blackwell Science, Oxford, UK, p. 379.
- Smigaj, W., Betcke, T., Arridge, S., Phillips, J., Schweiger, M., 2015. Solving boundary integral problems with BEM++. *ACM Trans. Math. Softw.* 41, 1–40. <https://doi.org/10.1145/2590830>.
- Sobradillo, B., Boyra, G., Pérez-Arjona, I., Martínez, U., Espinosa, V., 2021. Ex situ and in situ target strength measurements of European anchovy in the Bay of Biscay. *ICES J. Mar. Sci.* 78, 782–796. <https://doi.org/10.1093/icesjms/fsaa242>.
- Stanton, T.K., Chu, D., Jech, J.M., Irish, J.D., 2010. New broadband methods for resonance classification and high-resolution imagery of fish with swimbladders using a modified commercial broadband echosounder. *ICES J. Mar. Sci.* 67, 365–378.
- Yang, Y., Gastauer, S., Proud, R., Mangeni-Sande, R., Everson, I., Kayanda, R.J., Brierley, A.S., 2023. Modelling and in situ observation of broadband acoustic scattering from the Silver cyprinid (*Rastrineobola argentea*) in Lake Victoria, East Africa. *ICES J. Mar. Sci.* 10, 1–14. <https://doi.org/10.1093/icesjms/fsad137>.
- Yoon, E., Lee, H., park, K., Lee, Y.-D., Hwang, K., Kim, D.N., 2023. Ex situ target strength of yellow croaker (*Larimichthys polyactis*) in a seawater tank. *Fish. Res.* 106610. <https://doi.org/10.1016/j.fishres.2023.106610>.